Joint Special Interest Group meeting between euspen and ASPE
Advancing Precision in Additive Manufacturing
Inspire AG, St. Gallen, Switzerland 2021
www.euspen.eu

Quantifying the influence of local porosity on the colour differences of dyed laser sintered polyamide-12 with X-ray CT

S. Bellens[1], M. Janssens[1], T. Craeghs[1], P. Vandewalle[2], W. Dewulf[3]

[1]*Materialise NV, Technologielaan 15, Leuven, Belgium*
[2]*EAVISE, PSI, Dept. Of Electrical Engineering (ESAT), KU Leuven, Jan Pieter de Nayerlaan 5, Sint-Katelijne-Waver, Belgium*
[3]*Dept. Of Mechanical Engineering, KU Leuven, Celestijnenlaan 300, Heverlee, Belgium*

simon.bellens@materialise.be

Abstract
Aesthetic quality requirements for polymer laser sintered parts are becoming stricter to meet the high requirements of end-use applications. For laser sintered parts, several post-processing steps exist to improve the appearance of the parts, including sandblasting, tumbling or colouring. However, local changes in the porosity can influence the absorption of the colour dye and generate undesired colour differences. Test samples with altered build orientations are produced and post-processed by tumbling and colour dyeing. X-ray computed tomography is used to quantify the open and sub-surface porosity of the samples. The colour of the test samples is measured with an RGB colour camera. Device-dependent RGB values are converted to device-independent colour spaces (CIEXYZ and CIELAB), using a target-based colour characterization. Local ΔE* colour differences are calculated and aligned with 2D porosity maps of the open and sub-surface porosity. A strong correlation between the open pore volume and colour differences on the samples was observed.

Laser Sintering; Colour differences; Polyamide-12; X-ray Computed Tomography

1. Introduction

Polymer Laser Sintering (LS) is a versatile and flexible additive manufacturing (AM) technology to produce end-use functional parts. While the number of end-use applications is increasing, there still remain quality aspects that have to be addressed [1,2]. For end-use applications, the aesthetic quality requirements cannot be omitted and are becoming of equal importance as dimensional accuracy and material properties. Several post-processing steps exist, including sandblasting, tumbling, colouring or a combination of the previous, to improve the appearance of a part. For laser sintered parts, one can easily alter the colour of the part with colour dye methods due to the inherent porosity of the material [3]. Griessbach et al. proposed and patented a non-destructive immersion quality control procedure for LS PA12 parts [4]. The authors showed a strong correlation between the colour saturation and the measured porosity levels for PA12 LS parts. For higher porosity levels a higher colour saturation was observed [4]. However, it is not completely clear how deviations in the open and closed porosities alter the absorption of the materials and generate colour differences in the parts.
Spectrophotometers or colorimeters can easily measure the reflectance curves or colour of parts in a predefined colour space. However, the values represent an average value for a certain region and are difficult to register with the exact location on the parts. To obtain 2D colour information of objects, RGB colour cameras are frequently used [5,6]. The obtained RGB values are device dependent and have to be converted to a device-independent colour space (e.g. CIEXYZ and CIELAB). An in-depth explanation of camera characterization can be found in[7,8].

2. Methodology

To investigate the influence of open and closed porosities on the colour of the parts, ten test samples were printed, post-processed and colour dyed. The orientation of the samples was altered to create differences in the porosity levels near the surface. The test samples were scanned with X-ray computed tomography and analysed with a python script to determine the porosity levels. Thereafter, images of the test samples were obtained with a colour camera to measure the colour of the parts in the CIELAB colour space and to calculate ΔE^*_{00} colour differences. 2D porosity maps of the open and sub-surface pores were created from the XCT data and aligned with the CIELAB images. The same regions of interest were extracted from the 2D colour difference map and 2D porosity maps to study correlation between both.

2.1 Test samples

2.1.1 Production of the test samples

Cuboid samples with a size of 13x13x26 mm^3 were built in a state-of-the-art LS machine equipped with the Materialise Control Platform (MCP). PA2200 PA12 powder with a virgin and recycled power ratio of 50/50 was used. The test samples were consecutively rotated around the Z-axis (0 - 22.5 - 45 degrees) and X-axis (0 - 15 - 30 – 45 degrees). Table 1 lists the process parameters of the LS machine.

2.1.2 Post-processing of the test samples

After sand blasting, the test samples were tumbled for 8 hours and ultrasonically cleaned. Thereafter, the samples were colour dyed in a light brown colour with a pot dyeing procedure for 120 minutes. After dyeing, the parts were rinsed with water and

ultrasonically cleaned. Finally, the samples were dried in an oven at 60°C.

Table 1: LS process parameters to produce the test samples

General parameters	Value
Layer thickness	120 µm
Scan strategy	X-Y alternate
Contour parameters	
Laser power	45 W
Scan speed	4000 mm/s
Laser diameter	0,5 mm
Hatching parameters	
Laser power	60 W
Scan speed	6000 mm/s
Laser diameter	0,6 mm

2.2 Porosity measurements

2.2.1 X-ray computed tomography measurements

The test samples were scanned with a Nikon cone-beam computed tomography system. The cuboid samples were only partially scanned to achieve sufficient resolution in the XCT scans. Table 2 shows the settings of the XCT system. The settings were adopted from [2] to achieve a high Signal-to-Noise Ratio (SNR) and Contrast-to-Noise ratio (CNR) in the 3D reconstructions. VG studio MAX 3.4 was used to align the samples and to export regions of interest as 16-bit image stacks. Python code was used to analyse the XCT reconstructions and to calculate the open and closed porosity values.

Table 2: XCT settings to scan the test samples, adopted from [2]

Parameters	Value
Target Material	Molybdenum
X-ray source voltage	110 kV
X-ray source power	14 W
Detector exposure time	1415 ms
X-ray filter	None
Projections	3143
Magnification/Voxel size	18/0.011115 µm

2.2.2 Determine open and sub-surface porosity

The 16-bit grayscale image stacks are imported and processed as 3D arrays. Otsu's global segmentation algorithm was used to segment the 3D reconstruction [9]. Pores represented by less than 8 voxels were removed from the segmentation and assigned as material. The largest connected air region is separated from the pores and is considered as the background of the XCT scan. Thereafter, a 3D binary morphologic closing operation with a ball kernel with a radius of 15 voxels was applied on the segmented volume. The morphologic operation closes the open pores or valleys in the surface and thereby approximates the form of the surface [10]. The peaks or hills of the surface remain unaffected. The overlapping regions of the background and the morphologic closed volume therefore represent the open porosity of the material. Figure 1 shows the four main steps to determine the open porosity level.

Closed pores, connected regions completely encapsulated by the material, with a centre point within 200 µm from the original surface are considered as sub-surface pores. Other pores were excluded during the analysis. 2D porosity maps, inspired by [11], from the open and sub-surface pores were created from the 3D voxel models by counting the number of open or sub-surface voxels, respectively for each column.

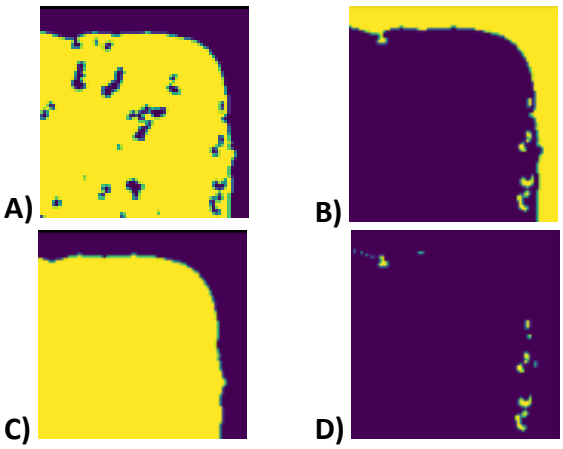

Figure 1: Four main steps to determine the open porosity of the test samples. A) Segmented volume with Otsu's global segmentation algorithm; yellow represents material, purple represent air. B) Background of the XCT (yellow). C) Morphologically closed volume. D) Open pores in the material, defined as the intersection between the background (B) and the morphologically closed volume (C). Note that air regions can be completely encapsulated in the 2D representation but are connected with the background in 3D.

2.3 Colour measurements

2.3.1 Camera setup

A Basler acA5472-17uc 20 MP camera, equipped with a Fujinon CF25ZA-1S lens with a fixed focal length of 25 mm, was positioned in a basic light booth (byko-spectra basic from BYK, see Figure 2). The output of the camera system are RGB images without white-balance correction or post-processing. The camera aperture and exposure time were set to achieve sufficient depth of view and avoid pixel saturation. Throughout the experiments, the D65 light source from the light cabin was used. The camera setup was positioned in a temperature (20 °C ± 0,5 °C) and relative humidity controlled metrology lab. To avoid the influence of surrounding light, the lights in the room are turned off during the acquisition of the images and no windows were present in the room. Before each measurement, the camera and lights were turned on for at least 60 minutes to reach a stable working condition.

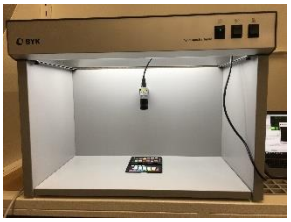

Figure 2: RGB colour camera mounted in a BYK light cabin

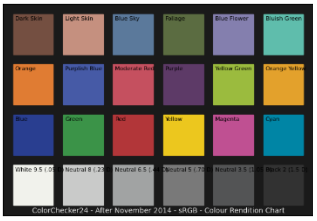

Figure 3: Render of a Macbeth ColorChecker chart (Classic X-rite chart)

2.3.2 Geometric calibration and distortion correction

To perform a geometric calibration of the camera system a checkerboard pattern with 12 by 13 square patches and a patch size of 4 mm was used. OpenCV implementations were used to detect the checkerboard corners with subpixel accuracy, perform the camera calibration and remove distortion from the acquired images. Approximately 25 images of the checkerboard were acquired to perform the geometric calibration and distortion correction. For the geometric calibration, a root mean square reprojection error of approximately 0,21 pixels was obtained.

2.3.3 Colour characterization of the camera

A colour characterization of the camera was performed to convert the device dependent RGB values to a device independent colour space (e.g. CIEXYZ). A target-based colour characterization was used to define a mapping between the device-dependent RGB values and device-independent CIEXYZ colour space. A classic X-rite ColorChecker with 24 target patches was used as a reference target and is shown in Figure 3. To compensate for differences in illumination of the target and the parts, a spatial correction was performed as described in [12]. From the spatially corrected image of the X-rite ColorChecker, the RGB values for the target patches were calculated as the average values from a region of interest of 100 by 100 pixels in each colour patch. Before the colour characterization, the linear response of the RGB colour camera was evaluated, using the 6 achromatic patches of the X-rite ColorChecker. A R^2 of at least 0.998 was obtained for each colour channel. Based on the measured RGB values from the camera and the target XYZ values, a mapping is created using the method as proposed by Cheung et al.[8]. The quality of the mapping between RGB and XYZ values was evaluated by calculating ΔE_{00}^* values after converting the obtained XYZ values to the CIELAB values. An average ΔE_{00}^* of 0,56 was obtained. The same conversion is then applied to the RGB images of the parts to obtain CIELAB images.

2.3.4 Alignment procedure colour images and XCT

Images of the parts were captured while the parts were positioned on the checkerboard. The corners of the checkerboard are detected to perform a 4-point perspective transformation on the images and compensate for possible tilt of the samples. Thereafter, the edges of the parts were detected using a canny edge detection algorithm. The distance between the edges was used to rescale the images from the camera images to the voxel size of the XCT scans. Consecutively, the edges of the parts were used align the camera images with the 2D porosity maps of the XCT measurements.

2.3.5 Colour differences

$$\Delta E^* = \sqrt{(\Delta L^*)^2 + (\Delta a^*)^2 + (\Delta b^*)^2} \quad (1)$$

In CIELAB colour space, a colour difference is defined as the Euclidean distance between the coordinates of two points in the colour space (equation 1) [12]. However, the latest definition according to CIEDE2000 was used to calculate the colour differences. The entire formula of the ΔE_{00}^* can be found in [12]. A ΔE_{00}^* value for each pixel in the CIELAB images of the parts was calculated while using the lightest observed colour as a reference. This implies that larger ΔE_{00}^* values belong to darker region in the parts

3. Results and Discussion

3.1 Microscopic images of the cross section

A microscopic image of the cross section was obtained after cutting, embedding and grinding the sample in consecutive steps. From Figure 4, one can observe the limited penetration depth of the colour dye, which is approximately 100 to 150 µm. Therefore, only open pores and sub-surface pores were considered as the main influencing factors to cause colour differences in the parts. For the microscopic images, a darker colour was preferred to obtain sufficient contrast between the colour dye and the material. Note also the large differences in penetration depth of the colour dye.

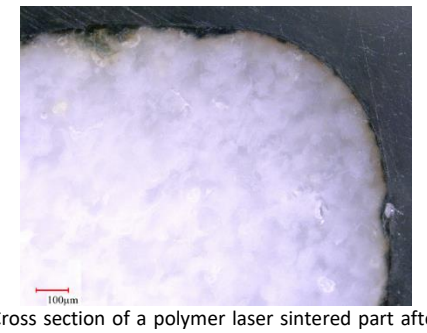

Figure 4: Cross section of a polymer laser sintered part after tumbling and colour dyeing with a dark green colour. A limited penetration depth of the dye and local deviations in the penetration depth can be observed.

3.2 Qualitative comparison between colour differences and porosity maps

Figure 5 shows a comparison between the calculated colour differences and the open and sub-surface porosity maps for two different sides of sample 1. For Side A, one can observe an increasing colour difference towards the right side of the part. In the porosity maps, one can also observe a slight increase in the open porosity level. While comparing the two sides of the object, larger colour differences and an increase in the open porosity level can be noticed. However, for the sub-surface porosity map the difference between both sides remains relatively small. A higher open porosity value is believed to result in a larger surface area, hence ability of the colour dye to penetrate the material. A higher absorption of the colour dye results in less reflection of the original white colour of the part and results in darker regions. As for Cube 01 no rotation around the X-axis and Z-axis was applied, the colours for both sides were expected to be the same. However, in the toolpath one can observe a larger distance between contour and hatching vectors for Side C. This results in a lower local energy density near the surface of Side C and immediately translates to a local increase in the porosity.

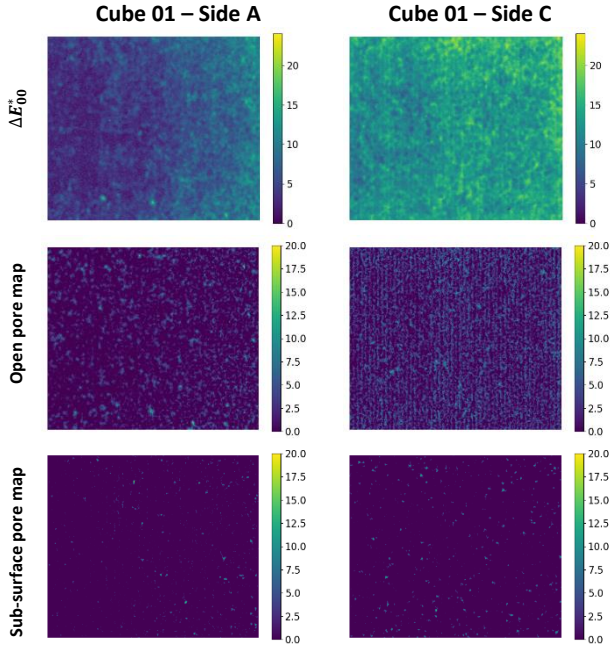

Figure 5: Colour difference maps, open and sub-surface porosity maps for Side A and Side C of Cube 01. Notice the large colour difference and variations in open porosity for both sides.

3.3 Quantitative comparison between colour differences and porosities

Regions of interest were cropped from the ΔE^*_{00} images and the 2D porosity maps of the parts. The average values and standard deviations for the region of interest in the ΔE^*_{00} images were calculated. The open and sub-surface pore volumes from the same region of interest were obtained by counting the number of porosity voxels of each category in the same region of interest and multiplying by the volume of one voxel. Figure 6 shows the average colour difference for 5 regions of interest of 200 by 200 pixels from one side of the 10 cubes against the calculated open pore volume. A clear correlation between both values was observed. A higher open pore volume results in a larger colour difference, hence darker colour of the test sample. This is observed in between the 5 regions for each cube as well in between the different cubes. Figure 7 shows the same colour differences against the sub-surface pore volume. Larger deviations in the porosity levels were observed and a lower correlation with the colour differences was obtained. Table 3 shows the Pearson correlation coefficient between the open and sub-surface pore volumes with different sizes for the regions of interest. A decreasing size of the region of interest results in a lower Pearson correlation coefficient. This is especially the case for sub-surface porosities. However, the Pearson coefficient remains rather high for open porosities which implies that the colour is mainly determined by the open porosity of the material and colour differences are caused by differences in the open porosity of the material.

4. Conclusion

Test samples with altered build orientations were printed, post-processed and colour dyed to create test samples with altered open and sub-surface porosity levels, hence part colour. The open and sub-surface porosity levels of the test samples were determined with X-ray computed tomography measurements and we derived 2D porosity maps of the open and sub-surface porosities. The parts were imaged with an RGB colour camera, which was characterized with a target-based colour characterization to achieve CIELAB images of the parts. The correlation of the open and sub-surface porosities and the colour differences was investigated. A strong correlation between the open porosity and colour differences was observed. A higher local open pore volume results in a higher colour difference, hence darker colour. To reduce or avoid undesired colour differences, the surface of the parts therefore has to be produced in a more consistent or stable way. Next steps can investigate alternative toolpaths and hereby increase the consistency of the local energy density and improve the stability of the open porosities near the surface of the parts.

Table 3: Pearson correlation coefficient calculated for the average colour difference in relation to the open and sub-surface pore volume.

Pearson correlation coefficient (R)	Region of interest size of 200 by 200 pixels	Region of interest size of 50 by 50 pixels
Open porosity	0.967	0.919
Sub-surface porosity	0.803	0.394

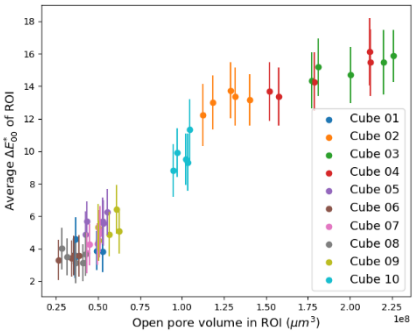

Figure 6: Colour differences for 5 regions of interest (ROI) with a size of 200 by 200 pixels for one side of the 10 cubes plotted against the open pore volume in the same ROI.

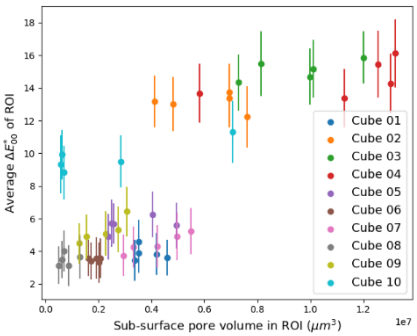

Figure 7: Colour differences for 5 regions of interest (ROI) with a size of 200 by 200 pixels for one side of the 10 cubes plotted against the sub-surface pore volume in the same ROI.

References

[1] R.D. Goodridge, C.J. Tuck, R.J.M. Hague, Laser sintering of polyamides and other polymers, Prog. Mater. Sci. 57 (2012) 229–267.

[2] M. Pavan, T. Craeghs, J.P. Kruth, W. Dewulf, Investigating the influence of X-ray CT parameters on porosity measurement of laser sintered PA12 parts using a design-of-experiment approach, Polym. Test. 66 (2018) 203–212.

[3] I. Gibson, D. Rosen, B. Stucker, Additive Manufacturing Technologies, 2015.

[4] S. Griessbach, R. Lach, W. Grellmann, Structure-property correlations of laser sintered nylon 12 for dynamic dye testing of plastic parts, Polym. Test. 29 (2010) 1026–1030.

[5] K. León, D. Mery, F. Pedreschi, J. León, Color measurement in L*a*b* units from RGB digital images, Food Res. Int. 39 (2006) 1084–1091.

[6] N.A. Valous, F. Mendoza, D.W. Sun, P. Allen, Colour calibration of a laboratory computer vision system for quality evaluation of pre-sliced hams, Meat Sci. 81 (2009) 132–141.

[7] G.D. Finlayson, M. Mohammadzadeh Darrodi, M. Mackiewicz, The alternating least squares technique for nonuniform intensity color correction, Color Res. Appl. 40 (2015) 232–

[8] V. Cheung, S. Westland, D. Connah, C. Ripamonti, A comparative study of the characterisation of colour cameras by means of neural networks and polynomial transforms, Color. Technol. 120 (2004) 19–25.

[9] N. Otsu, A Threshold Selection Method From Gray-Level Histograms., IEEE Trans Syst Man Cybern. SMC-9 (1979) 62–66.

[10] S. Lou, X. Jiang, P.J. Scott, Applications of morphological operations in surface metrology and dimensional metrology, J. Phys. Conf. Ser. 483 (2014).

[11] W. Dewulf, M. Pavan, T. Craeghs, J.P. Kruth, Using X-ray computed tomography to improve the porosity level of polyamide-12 laser sintered parts, CIRP Ann. - Manuf. Technol. 65 (2016) 205–208.

[12] M.A. Kriss, L.W. Macdonald, M.D. Fairchild, Computational colour science using MATLAB, 2012.